Transmural Ventricular Heterogeneities Play a Major Role in Determining T-Wave Morphology at Different Extracellular Potassium Levels

Hassaan A Bukhari[1,2,4,5], Flavio Palmieri[2,3], Dina Ferreira[8], Mark Potse[4,5], Julia Ramírez[6], Pablo Laguna[1,2], Carlos Sánchez[1,2,7], Esther Pueyo[1,2]

[1] BSICoS group, I3A Institute, University of Zaragoza, IIS Aragón, Zaragoza, Spain
[2] CIBER en Bioingeniería, Biomateriales y Nanomedicina (CIBER-BBN), Zaragoza, Spain
[3] Centre de Recerca en Enginyeria Biomèdica, Universitat Politècnica de Catalunya, Barcelona, Spain
[4] Carmen team, Inria Bordeaux Sud-Ouest, Talence, France
[5] University of Bordeaux, IMB, UMR 5251, Talence, France
[6] William Harvey Research Institute, Queen Mary University of London, London, United Kingdom
[7] Defence University Centre (CUD), General Military Academy of Zaragoza (AGM), Zaragoza, Spain
[8] Laboratorios Rubio, Castellbisbal, Barcelona, Spain

Abstract

End-stage renal disease (ESRD) affects more than 10% of the world population. ESRD patients present impaired potassium homeostasis, which increases the risk for ventricular arrhythmias and sudden cardiac death. Non-invasive estimation of serum potassium, $[K^+]$*, before the patient experiences serious consequences is of major importance. In this study, we investigated the relationship of* $[K^+]$ *with three T-wave morphological descriptors: the T-wave width (*T_w*), slope-to-amplitude ratio (*T_{SA}*) and temporal morphological variability (*d_w*) from ECGs of 12 ESRD patients undergoing hemodialysis and from simulated ECGs. Spearman's correlation coefficients between the descriptors* T_w*,* T_{SA} *and* d_w *and* $[K^+]$ *were* -0.5*, 0.8 and 0.65, respectively. These associations were, however, highly patient-dependent. The high inter-individual variability in T-wave morphology, particularly observed at high* $[K^+]$*, was reproduced in the simulations and could be explained by differences in transmural heterogeneities, with 10% variations in the proportion of midmyocardial cells leading to changes larger than 15% in T-wave morphology. In conclusion, T-wave morphological descriptors have the potential to be used as predictors of* $[K^+]$ *in ESRD patients, but their associated inter-individual variability should be taken into account, especially under hyperkalemic conditions.*

1. Introduction

End-stage renal disease (ESRD) represents a global health burden, with an estimated 10% of the worldwide population being affected. This involves high associated economic cost, increased mortality risk, and decreased quality of life for affected patients [1]. As renal function declines, ESRD patients present an increasingly impaired ability to maintain potassium homeostasis. Serum potassium levels ($[K^+]$) outside normal ranges, in the form of hypokalemia or hyperkalemia, increase the risk for life-threatening arrhythmias and sudden cardiac death [2]. Investigating the effects of $[K^+]$ variations on the electrical functioning of the heart could help improve therapies and risk stratification tools, for example by using the ECG to continuously monitor $[K^+]$.

Variations of $[K^+]$ levels have been shown to affect depolarization and repolarization features of the ECG in previous studies [3–5], suggesting that indeed it is possible to infer $[K^+]$ from the ECG. However, in patient data we found a wide variety of relations between $[K^+]$ and repolarization characteristics in the ECG. These repolarization features are also influenced by the dispersion of repolarization properties in the heart. Therefore we hypothesized that the inter-individual differences in the relation between $[K^+]$ and ECG features can be caused by inter-individual differences in the dispersion of primary repolarization properties. We simulated a set of ventricular fibers covering a wide range of transmural heterogeneities and we calculated pseudo-ECGs at different $[K^+]$. We characterized the simulated T-wave morphology changes by using three descriptors (T_w, T_{SA}[6] and d_w[7]) and we compared them with those from ECGs of patients undergoing hemodialysis (HD), i.e. experiencing large $[K^+]$ variations. Upon confirmation of the model's ability to reproduce inter-individual variability in the evaluated T-wave descriptors, we performed a sensitivity analysis to assess the dependence of T-wave morphology descriptors

 ISSN: 2325-887X DOI: 10.22489/CinC.2019.404

on transmural heterogeneities and assess whether transmural dispersion indeed contributes to explain inter-individual differences in T-wave morphology, particularly for $[K^+]$ values out of normal ranges.

2. Methods

Clinical Measurements The study population included 12 ESRD patients from Hospital Clínico Universitario de Zaragoza (HCUZ). 48-hour 12-lead ECGs were acquired at a sampling frequency of 1 kHz and amplitude resolution of 3.75 μV (H12+, Mortara Instruments, Milwaukee, WI, USA). The acquisition started 5 minutes before the HD treatment onset and lasted for 48 hours (Figure 1 bottom blue line). Simultaneously, six blood samples were taken and analyzed during the HD session: the first one at the HD onset and the next three samples every hour during the HD session (Figure 1, K1 to K4 in red). The $5th$ blood sample was collected at the end of the HD (minute 215 or 245, depending on the patient) while the $6th$ blood sample was taken after 48 hours, immediately before the next HD session. Extracellular potassium concentrations, $[K^+]$, were measured at those time points, as shown in Figure 1. The ethical committee approved the study protocol, with all patients providing signed informed consent.

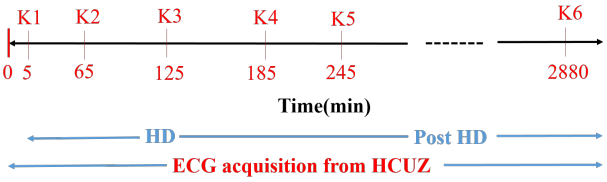

Figure 1. Diagram of the study protocol. K1 to K6 are the time points (in minutes) for blood sample extraction.

The measured ECG signals were band-pass filtered (0.5 to 40 Hz) to remove baseline wander, muscular noise, and powerline interference. QRS detection and wave delineation were performed by using a wavelet-based single-lead delineation method [8]. To emphasize T-wave components while allowing more accurate delineation, Principal components (PCs) were obtained by computing the auto-correlation matrix of T-waves in a stable ECG segment at the end of the HD session. The ECG recording was subsequently projected into the direction of the 1st PC. The T-waves in the obtained 1st PC were delineated [8] and used for further analysis. In simulated pECGs, single-lead wavelet-based delineation was directly applied over the signals. The onset, peak, and end of the T-wave were determined.

Computational Modeling Transmural electrical propagation from ventricular endocardium to epicardium was simulated using 1-dimensional fibers (1.65 cm). A train of 10 stimuli was applied to the first cell of the fiber every 1000 ms with an amplitude equal to 1.5 times the diastolic threshold. Cellular electrophysiology was represented by a modified version of the O'Hara model [9] for the human ventricular action potential, as described by Dutta et al. [10]. To compute electrical propagation, a finite element method-based software [11] was used with a time step of 0.5 ms and space discretization of 0.01 cm. Intracellular and extracellular conductivities in the fiber were adjusted to obtain a conduction velocity of 44 cm/s.

Different proportions of endo-, mid- and epicardial cells were simulated for a total of 19 combinations: endocardial layer ranging from 10% to 50%, midmyocardial layer from 10% to 40% and epicardial layer from 20% to 80%. We use the notation CXYZ, where C stands for the word "case" and X, Y and Z denote the first digit of the proportions of endocardial, midmyocardial and epicardial cells, respectively (e.g. C532 represents the case with 50%, 30% and 20% of endocardial, midmyocardial and epicardial cells, respectively).

Pseudo-electrocardiogram signals (pECGs) were computed using equation (1) as described by Gima et al. [12]:

$$V_e = \epsilon \int \nabla V_m \cdot (\nabla \frac{1}{r})\, dr, \qquad (1)$$

where ϵ is a constant proportional to the ratio of intracellular and extracellular conductivities, V_m is the transmembrane potential and r is the distance between each cell in the fiber and the virtual electrode located 2 cm away from the last epicardial cell in the fiber direction.

Simulations for each ventricular fiber and associated pECGs were run for five different values of $[K^+]$, which included the reference physiological level in the O'Hara model, i.e. $[K^+]$ = 5.4 mmol/l, as well as two levels below and two above it: $[K^+]$ = 2, 3, 5.4, 7, 8 mmol/l.

T-wave Morphology Characterization The following T-wave morphological descriptors were studied:

- T_w, representing the width of the T-wave from T-wave onset to T-wave end;
- T_{SA}, representing the ratio between the T-wave downward slope and amplitude, calculated as in [6]; and
- d_w, representing temporal variations in T-wave morphology [7] (Figure 2).

d_w was computed considering as a reference T-wave the T-wave measured at physiological $[K^+] = 5.4$ mmol/L in the simulations and the T-wave measured at the end of the HD session in ESRD patients. Let's now consider the T-wave for a given $[K^+]$ (mmol/L), $\boldsymbol{f}^s(\boldsymbol{t}^s) = [f^s(t^s(1)), ..., f^s(t^s(N_s))]^\top$, and the reference T wave, $\boldsymbol{f}^r(\boldsymbol{t}^r) = [f^r(t^r(1)), ..., f^r(t^r(N_r))]^\top$, where $\boldsymbol{t}^r = [t^r(1), ..., t^r(N_r)]^\top$ and $\boldsymbol{t}^s = [t^s(1), ..., t^s(N_s)]^\top$ and N_r and N_s are the total durations of $\boldsymbol{t}^r$ and $\boldsymbol{t}^s$. Figure 2 (top left panel) shows $\boldsymbol{f}^r$ and $\boldsymbol{f}^s$, with their respective time domains, $\boldsymbol{t}^r$ and $\boldsymbol{t}^s$. Let $\gamma(\boldsymbol{t}^r)$ be the warping function that

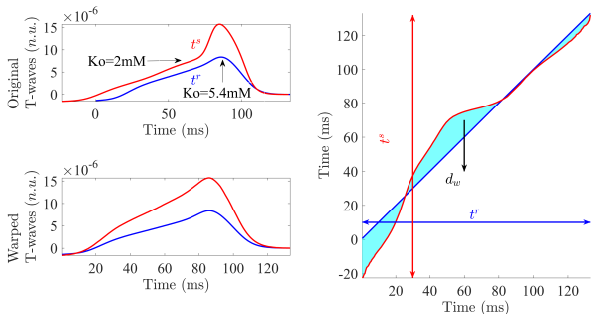

Figure 2. Time warping analysis for simulated fiber C118. Top left panel shows reference (blue) and studied (red) T-waves aligned with respect to their gravity centers. The blue area in the right panel represents d_{w}. Bottom left panel depicts the final warped T-waves.

relates $\boldsymbol{t}^r$ and $\boldsymbol{t}^s$, such that $\boldsymbol{f}^s(\gamma(\boldsymbol{t}^r))$ denotes the time-domain warping of $\boldsymbol{f}^s(\boldsymbol{t}^s)$ using $\gamma(\boldsymbol{t}^r)$. The square-root slope function (SRSF) transformation is defined as:

$$\boldsymbol{q}_f(\boldsymbol{t}) = \mathrm{sign}(\dot{\boldsymbol{f}}(\boldsymbol{t}))\,|\dot{\boldsymbol{f}}(\boldsymbol{t})|^{\frac{1}{2}}. \tag{2}$$

The optimal warping function is the one that minimizes the SRSF amplitude difference:

$$\gamma^*(\boldsymbol{t}^r) = \underset{\gamma(\boldsymbol{t}^r)}{\arg\min}\left(\left\|\boldsymbol{q}_{f^r}(\boldsymbol{t}^r) - \boldsymbol{q}_{f^s}(\gamma(\boldsymbol{t}^r))\sqrt{\dot{\gamma}(\boldsymbol{t}^r)}\right\|\right). \tag{3}$$

A dynamic programming algorithm was used to obtain the optimal warping function, $\gamma^*(\boldsymbol{t}^r)$, that optimally warps $\boldsymbol{f}^r(\boldsymbol{t}^r)$ and $\boldsymbol{f}^s(\boldsymbol{t}^s)$, which is shown in Figure 2 (right panel). The warped T-wave, $\boldsymbol{f}^s(\gamma^*(\boldsymbol{t}^r))$, is shown in Figure 2 (bottom left panel), together with the reference T-wave, $\boldsymbol{f}^r(\boldsymbol{t}^r)$.

The descriptor d_w (Figure 2, right panel) quantifies the level of warping required to optimally align two T-waves:

$$d_w = \left(\frac{s_d}{|s_d|}\right)\frac{1}{N_r}\sum_{n=1}^{N_r}|\gamma^*(t^r(n)) - t^r(n)|, \tag{4}$$

where $s_d = \sum_{n=1}^{N_r^u}(\gamma^*(t^r(n)) - t^r(n))$ is used to account for the sign estimated at the N_r^u T-wave upslope samples.

Sensitivity Analysis To assess how the proportion of endo-, mid- and epicardial cells modulated T-wave morphology descriptors at different $[\mathrm{K}^+]$, a sensitivity analysis was performed. For each T-wave descriptor, the percentage of change and its sensitivity to changes in the proportion of cells of each ventricular layer were computed as follows [13]:

$$D_{m;p;a_{\mathrm{i}}} = \left(\frac{M_{p;a_{\mathrm{i}}} - M_{\mathrm{control}}}{M_{\mathrm{control}}}\right)\times 100, \quad i = 1,2 \tag{5}$$

$$S_{m;p;a1,a2} = \left(\frac{D_{m;p;a_2} - D_{m;p;a_1}}{a_2 - a_1}\right)\times 100 \tag{6}$$

where $M_{\mathrm{p;a}}$ is the value of the T-wave descriptor (m) under a varying proportion a of cells in the analyzed layer (p) calculated at proportions a_1 and a_2. M_{control} is the value of the T-wave descriptor at the default proportion of cells in the layer, this being 30, 30 and 40% for endocardial, midmyocardial and epicardial cells, respectively.

3. Results and Discussion

Figure 3 illustrates the results of the T-wave characterization for one of the ventricular fibers simulated in this study. Panel (a) shows the aligned T-waves corresponding to $[\mathrm{K}^+]$ ranging from 2 to 8 mmol/L. Panels (b), (c) and (d) show the relationship between each of T_{w}, T_{SA} and d_{w} and $[\mathrm{K}^+]$, respectively. $[\mathrm{K}^+]$ elevation leads to a reduction in the T-wave duration, an increase in the ratio between T-wave slope and amplitude and enhancement of T-wave temporal morphological variability.

Figure 4 illustrates the T-wave descriptors T_{w}, T_{SA} and d_{w} for four simulated fibers (top Panel (a)) and four patients of the study population (bottom panel (b)) as a function of $[\mathrm{K}^+]$, respectively. Although the three T-wave morphology descriptors are correlated with $[\mathrm{K}^+]$ (median Spearman's correlation coefficients of -0.5, 0.8 and 0.65), a diversity of patterns in the three relationships is apparent, both in simulated and patients' ECGs.

Figure 5 shows the results from the sensitivity analysis for T_{SA}. Analogous results were obtained for T_{w} and d_{w}. As can be observed, the largest sensitivity of T_{SA} was found to variations in the proportion of midmyocardial cells within the ventricular wall. This was particularly more prominent when $[\mathrm{K}^+]$ became elevated above physiological levels. For $[\mathrm{K}^+]$ = 8 mmol/l, sensitivity values above 150% were found, which means that 10% variations in the midmyocardial proportion led to changes larger than 15% in T_{SA} (similarly for the other T-wave descriptors).

Descriptors of T-wave width, amplitude-to-slope ratio, and temporal morphological variability were shown to vary with $[\mathrm{K}^+]$ in both simulated and measured ECGs, but a wide range of patterns was observed for such relationships. The proportion of midmyocardial cells within the simulated ventricular fibers has a large impact on T-wave morphology descriptors, particularly under elevated $[\mathrm{K}^+]$. This suggests that transmural heterogeneities can have a relevant role in predicting the patient-specific response of ventricular repolarization to hyperkalemia.

Acknowledgements

This work was supported by projects ERC-2014-StG 638284 (ERC), DPI2016-75458-R (MINECO), Marie Skłodowska-Curie grant 764738 and Aragón Government

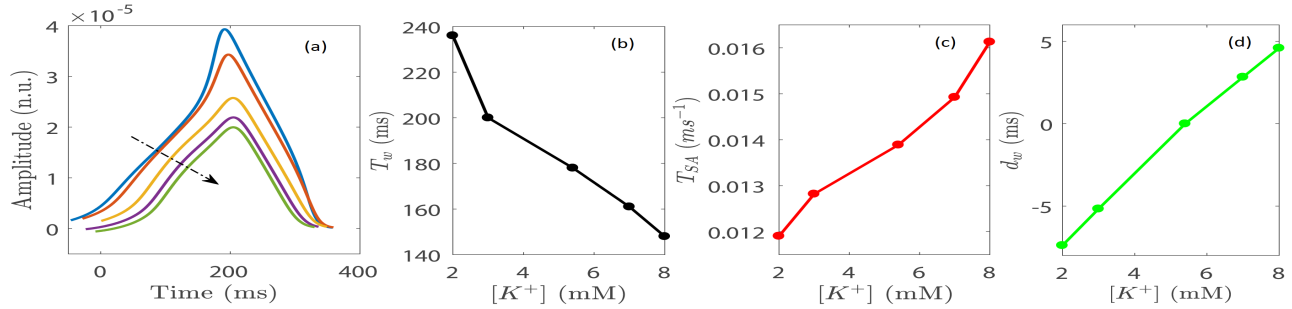

Figure 3. T-waves and T_{w}, T_{SA} and d_{w} evaluated for simulated fiber C145 under varying $[\mathrm{K}^+]$. The arrow in the left panel indicates the direction of increasing $[\mathrm{K}^+]$ from 2 to 8 mmol/L.

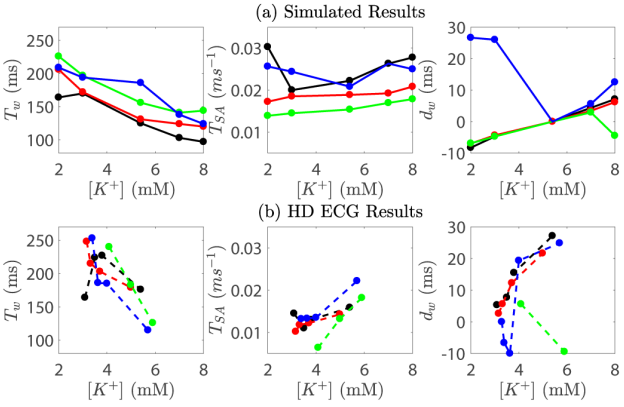

Figure 4. T_{w}, T_{SA} and d_{w} for simulated fibers C118, C127, C136 and C532 and patients HCUZP1, HCUZP4, HCUZP8 and HCUZP15 at varying $[\mathrm{K}^+]$.

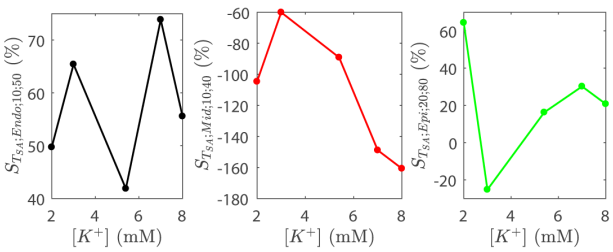

Figure 5. Sensitivity analysis for T_{SA} to variations in the proportion of endocardial (left), midmyocardial (middle) and epicardial (right) layers at varying $[\mathrm{K}^+]$.

(Reference Group BSICoS T39-17R) cofunded by FEDER 2014-2020. JR acknowledges support from EU H2020 under Marie Sklodowska-Curie grant 786833.

References

[1] Hill NR, et al. Global prevalence of chronic kidney disease a systematic review and meta-analysis. PLoS ONE July 2016;11(7):e0158765.

[2] Weiss JN, et al. Electrophysiology of hypokalemia and hyperkalemia. Circ Arrhythm Electrophysiol Mar. 2017;10:1–10.

[3] Lanari A, et al. Electrocardiographic effects of potassium. I. Perfusion through the coronary bed. Am Heart J Mar. 1964;67(3):357–363.

[4] El-Sherif N, et al. Electrolyte disorders and arrhythmogenesis. Cardiol J 2011;18(2):233–245.

[5] Mieghem C, et al. The clinical value of the ECG in noncardiac conditions. Chest Apr. 2004;125(4):1561–1576.

[6] Corsi C, et al. Validation of a novel method for non-invasive blood potassium quantification from the ECG. Computers in Cardiology Sep. 2012;39:105–108.

[7] Ramírez J, et al. Variability of ventricular repolarization dispersion quantified by time-warping the morphology of the T-wave. IEEE Trans Biomed Eng Jul 2017;64(7):1619–1630.

[8] Martínez JP, et al. A wavelet-based ECG delineator: Evaluation on standard databases. IEEE Trans Biomed Eng Apr. 2004;4(51):570–581.

[9] O'Hara T, et al. Simulation of the undiseased human cardiac ventricular action potential: model formulation and experimental validation. PLoS Comput Biol May 2011; 7(5):e1002061.

[10] Dutta S, et al. Electrophysiological properties of computational human ventricular cell action potential models under acute ischemic conditions. Progress in Biophysics and Molecular Biology Oct. 2017;129:40–52.

[11] Heidenreich EA, et al. Adaptive macro finite elements for the numerical solution of monodomain equations in cardiac electrophysiology. Ann Biomed Eng Mar. 2010; 38(7):2331–45.

[12] Gima K, et al. Ionic current basis of electrocardiographic waveforms a model study. Circ Res May 2002;90(8).

[13] Romero L, et al. Impact of ionic current variability on human ventricular cellular electrophysiology. Am J Physiol Heart Circ Physiol Oct. 2009;297(4):1436–1445.

Address for correspondence:

Hassaan A. Bukhari; Institute of Engineering Research of Aragón, Universidad de Zaragoza (Spain).
hassaanahmed01@unizar.es